Research article

Yue Fu, Rashid A. Ganeev*, Ganjaboy S. Boltaev, Sandeep Kumar Maurya, Vyacheslav V. Kim, Chen Zhao, Anuradha Rout and Chunlei Guo*

Low- and high-order nonlinear optical properties of Ag_2S quantum dot thin films

https://doi.org/10.1515/nanoph-2018-0213
Received December 4, 2018; revised February 28, 2019; accepted March 4, 2019

Abstract: Thin films containing small-sized quantum dots (QDs) and nanoparticles have shown strong optical nonlinearities caused by the confinement effect. Here, we report the study of third-order optical nonlinearities of silver sulfide (Ag_2S) QD thin films using 800 and 400 nm, 30 fs pulses. The absorption spectrometry and transmission electron microscopy are used to characterize the synthesized 80 and 500 nm Ag_2S QD films. The giant enhancement of nonlinearities is observed up to three to six orders of magnitude larger compared to those for the bulk and liquid Ag_2S samples. We also demonstrate the efficient high-order harmonic generation in the plasmas produced during ablation of the Ag_2S QD thin films. The analysis of the dynamics of the QD-containing plasma spreading allowed optimization of the delay between the heating and the driving pulses for an enhancement of harmonics conversion efficiency.

***Corresponding authors: Rashid A. Ganeev,** The Guo China-US Photonics Laboratory, State Key Laboratory of Applied Optics, Changchun Institute of Optics, Fine Mechanics and Physics, Chinese Academy of Sciences, Changchun 130033, P.R. China; and Physical Faculty, Voronezh State University, Voronezh 394006, Russia, e-mail: rashid@ciomp.ac.cn; and **Chunlei Guo,** The Guo China-US Photonics Laboratory, State Key Laboratory of Applied Optics, Changchun Institute of Optics, Fine Mechanics and Physics, Chinese Academy of Sciences, Changchun 130033, P.R. China; and The Institute of Optics, University of Rochester, Rochester, NY 14627, USA, e-mail: guo@optics.rochester.edu
Yue Fu: The Guo China-US Photonics Laboratory, State Key Laboratory of Applied Optics, Changchun Institute of Optics, Fine Mechanics and Physics, Chinese Academy of Sciences, Changchun 130033, P.R. China; and University of Chinese Academy of Sciences, Beijing 100039, P.R. China. https://orcid.org/0000-0002-9767-1868
Ganjaboy S. Boltaev, Sandeep Kumar Maurya, Vyacheslav V. Kim, Chen Zhao and Anuradha Rout: The Guo China-US Photonics Laboratory, State Key Laboratory of Applied Optics, Changchun Institute of Optics, Fine Mechanics and Physics, Chinese Academy of Sciences, Changchun 130033, P.R. China

Keywords: Ag_2S; high harmonics generation (HHG); nonlinear absorption and refraction; quantum dot films.

1 Introduction

Recently, significant efforts were made in the syntheses of metal chalcogenide nanocrystals (NCs) due to their attractive size-tunable optical properties and possible applications in various technological fields including light-emitting diodes [1, 2], photovoltaic devices [3, 4], and fluorescent biological labels [5, 6]. Several other sulfide precursors were subsequently reported, but elemental sulfur is most widely used as a less air-sensitive precursor in the syntheses of metal sulfide NCs. Decreasing the size of such materials allows us to tune their physical properties and observe new phenomena. The band gap (E_g) of quantum dots (QDs) increases by decreasing their size and the quantum confinement effect can strongly enhance the third-order optical nonlinearity. The QDs have interesting characteristics such as fluorescence photosensitivity and large optical nonlinearities: the electronic states of QDs are strongly influenced by the quantum confinement effect when the radius of QDs is smaller than approximately three times of the exciton Bohr radius [7]. The bulk semiconductor silver sulfide (Ag_2S) has the direct band gap $E_g = 1.0$ eV at 300 K and Bohr radius of the bulk material is not found [8]. Taking this into account, the newly synthesized semiconductor nanoparticles (NPs) should be studied under different conditions to understand the nonlinear optical mechanisms and use their attractive properties for practical applications [9–11].

Quantum dots thin films of different materials have also attracted much attention due to their various promising applications of solar cells and thin-film transistors [12–17]. Analyses of linear and nonlinear optical features of the thin films comprising metal sulfide NCs is important for their possible use in various fields of optoelectronics and laser physics. The size of the particles in the QDs film is smaller than the normal polycrystalline films. To verify the generalized effective-medium theories for linear and

nonlinear optical properties of metal sulfide NP and QDs requires the knowledge of linear and nonlinear susceptibilities of the constituent materials Ag_2S. QDs are noncadmium and nonlead fluorescent nanomaterials developed in recent years, and Ag_2S QDs are known for displaying large optical nonlinearities [18–20]. Ag_2S QD thin films can have even higher nonlinearities.

The QDs can also be efficiently used as the sources of high harmonics generation (HHG). HHG in gases, plasmas, and solids was extensively studied due to its possible applications in the generation of attosecond laser pulses and formation of short-wavelength coherent sources [21–30]. Note that the size variation of the polyatomic systems like QDs can efficiently manipulate the HHG spectra. By using HHG in atomic and molecular system, theory and experiment have come together to explore orbital tomography, molecular vibrational and dissociative dynamics, attosecond hole dynamics and many other interesting effects. At short distances from the target (<1 mm), atomic species are mostly responsible for HG at early times (<500 ns), while clusters and nanoaggregates mostly contribute at longer times (>1 μs). With the different HG times, HG becomes a powerful and universal technique for ablation plasma diagnosis and a tool to determine the nonlinear optical susceptibility of ejected clusters or NP [31].

In this study, we report on the variation of optical nonlinearities of Ag_2S QD thin films of different thickness. We also analyze the ablation of Ag_2S QD films for efficient emission of high-order harmonics of femtosecond pulses. Particularly, we demonstrate HHG using the electronically driven delay between the heating and the driving lasers for generation of harmonics from Ag_2S QD-contained plasmas in the range of 30–80 nm.

2 Experimental arrangements

In the typical process of synthesis 17 g $AgNO_3$ was dissolved in 100 ml tri-n-octyl-phosphine (TOP) to obtain the 1 M Ag-TOP. Some 6.4 ml of oleic acid, 5.4 g of 1-octadecylamine (ODA), and 12.8 ml of 1-octadecene were mixed in a 100 ml round-bottom flask under N_2 flushing three times to remove the water and oxygen and heated up to 70°C. With the continuous N_2 supply and stirring, 72 mg of sulfur powder was added into the flask immediately and heated to the temperature of 190°C. Then 4 ml of Ag-TOP was quickly injected in the flask, and the reaction was allowed to proceed for 5 min at 160°C. Some 10 ml of N-butyl alcohol was injected to provide solidification from ODA. The synthesized QDs were isolated by precipitation with methyl alcohol and redispersed in methylbenzene. This process was repeated three times to ensure a clean product. The obtained QDs dispersed in hexane or toluene was rinsed by ultrasonic process to achieve better dispersion of QDs (Aladin, Shanghai, China). The Ag_2S QD solution was then spin-coated on the glass slides to produce films of different thickness (80 and 500 nm). The thickness of the samples was measured using atomic force microscopy (Bruker, Billerica, MA, USA).

In order to study the low-order nonlinear optical properties of these two films we employed the single-beam Z-scan technique [32]. Ti:sapphire laser (Spitfire Ace, Spectra-Physics: 800 nm wavelength, 30 fs pulse duration, 1 kHz repetition rate) was used in these studies. The schematic diagram of the experimental setup is shown in Figure 1A. We also analyzed the nonlinear optical properties of films using the second harmonic of this radiation ($\lambda = 400$ nm).

Before the Z-scan measurements we analyzed the spatial characteristics of the probe beam using a CCD camera (Thorlabs, Shanghai, China) and confirmed that the beam profile in the focal area was close to Gaussian, which is a prerequisite for the analysis of Z-scan traces using the relations developed for this technique. The full width of focused femtosecond beams at $1/e^2$ level of intensity distribution was measured to be 72 μm. Before measuring the signal using a large area photodetector (Thorlab, Shanghai, China) with an aperture in front of it [closed-aperture (CA) scheme with 1 mm aperture allowing propagation of ~10% of output radiation and open-aperture (OA) scheme with fully opened aperture], we also used a detector to measure the incident pulse energy. The measurements of propagated radiation allowed determination of the nonlinear refractive indices (γ) and the nonlinear absorption coefficients (β) of our samples. The CA scheme allowed calculation of the sign and magnitude of γ and β of our films. The OA Z-scan was used for the measurements of β, which were compared with the measurements of this parameter using the CA scheme.

The transient absorption (TA) measurements were carried out using the noncollinear pump-probe technique at $\lambda = 400$ nm. The schematic of experimental setup is shown in Figure 1B. The femtosecond pulse ($\lambda = 800$ nm, $t = 30$ fs) was split at the ratio of 30:70 for the pump and probe pulses. The β-barium borate crystals were used to generate the 400 nm pump and probe radiation. These two pulses were focused on the Ag_2S QD thin film using a 300 mm focal length lens. The energies and beam waists of the pump and the probe pulses at the focus were adjusted to be 10:1 and 1:2, respectively, to match the condition required for observation of TA. In order to introduce the delay in arrival time of probe pulses with respect to pump pulses the former radiation was reflected by a pair of mirrors mounted on the motorized translational stage.

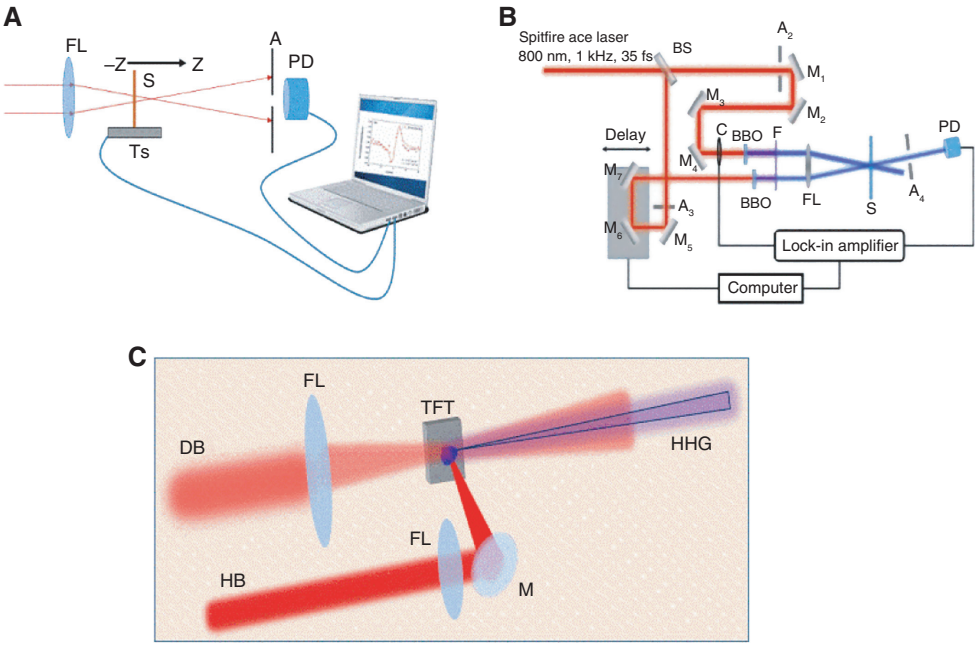

Figure 1: Experimental setup.
(A) Experimental setup for the measurement of the low-order nonlinear optical characteristics of the films. (B) Transient absorption experimental setup. FL, focusing lens; S, sample; Ts, translation stage; A, aperture; PD, photo detector; F, filter; M, mirror; BS, beam splitter; BBO, β-barium borate crystal. (C) High harmonics generation (HHG) setup. DB, driving beam; HB, heating beam; FL, focusing lenses; M, mirror; TFT, thin film target; HHG, HHG beam.

The arrival time of probe pulses with respect to pump pulses was controlled by moving the motorized translational stage connected to motion controller. The fast photodiode and lock-in-amplifier were used to measure the transmittance of the probe pulses with respect to the position of the motorized stage. Lock-in-amplifier was externally triggered by an optical chopper running at 300 Hz.

The Ti:sapphire femtosecond laser and Nd:YAG nanosecond laser were used in HHG studies (Spectra-Physics, Spitfire Ace, Santa Clara, CA, USA). The nanosecond Nd:YAG laser operating (LT100-A, Focus Medical LLC, USA) at 10 Hz pulse repetition rate is advantageous for plasma formation compared with the earlier used picosecond pulses. The nanosecond pulses allow formation of less ionized and less excited plasma during longer period of laser-matter interaction compared with shorter pulses. Additionally, the delay between the heating and the driving pulses could be electronically adjusted in broad range (0–10^6 ns), contrary to the earlier used optically driven delay.

The driving femtosecond pulses (800 nm, 30 fs, 1 kHz) propagated through the plasma produced on the Ag_2S NP film at different delays from the beginning of target irradiation by nanosecond heating pulses (1064 nm, 5 ns, 10 Hz; Q-smart, coherent). The variable delay between heating and driving pulses was established to generate harmonics in plasma at the used geometry of experiments, when the 800 nm femtosecond pulses were focused onto the area of plasma orthogonally to ablating radiation, at a distance of ~200 μm above the target surface (Figure 1C). The harmonics yield was maximized by adjusting the position of the target with regard to the optical axis of propagation of the driving femtosecond pulses and by varying the position of focus for this radiation with regard to the plasma. The harmonics emission was directed to the extreme ultraviolet (XUV) spectrometer containing a cylindrical mirror and a 1200 grooves/mm flat field grating with variable line spacing. The XUV spectrum was recorded by a microchannel plate with phosphor screen, and the harmonics were imaged by a CCD camera (Hamamatsu, Japan).

3 Results

3.1 Z-scans and TA measurements of Ag_2S QD films

Figure 2A shows the absorption spectra of two QD films of different thickness (80 and 500 nm). The absorption band between 300 and 400 nm (>2.0 eV) can be ascribed to the band gap of the Ag_2S QDs, which was blue-shifted compared with that of bulk Ag_2S (0.9 ~ 1.1 eV) [33]. The absorption

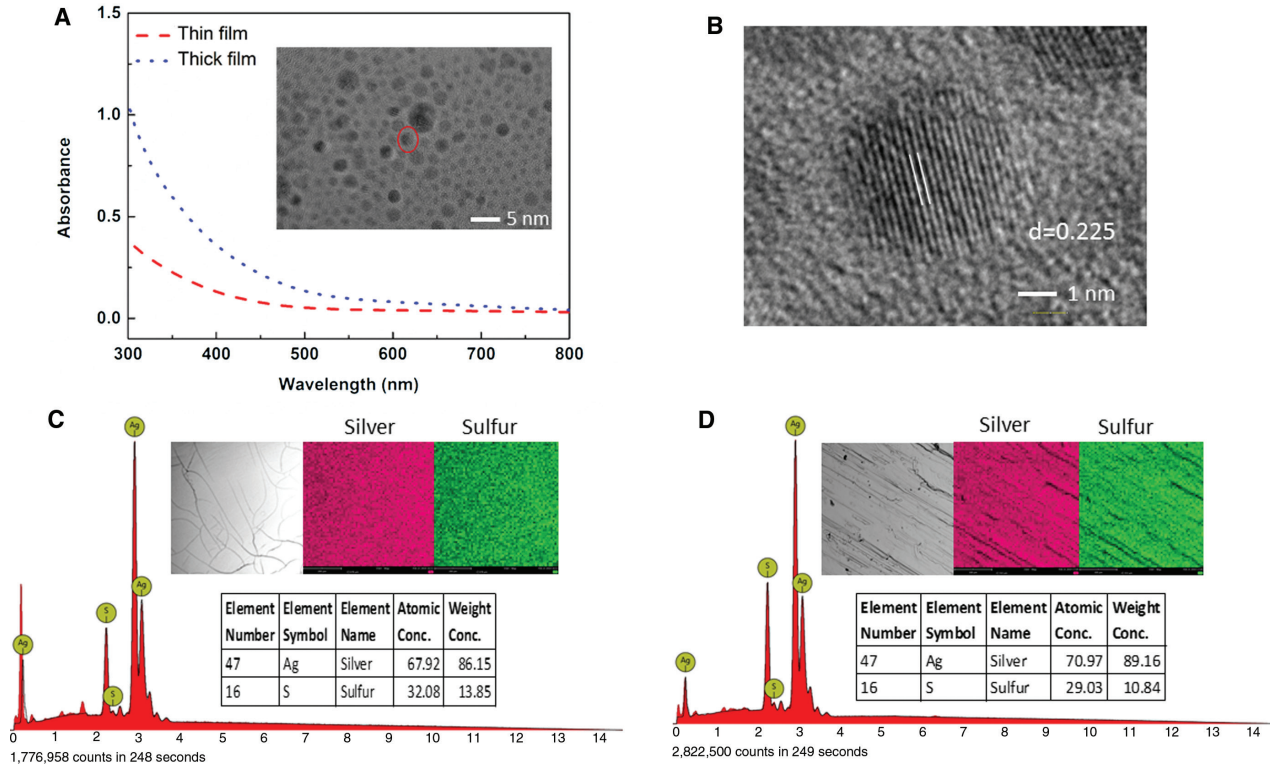

Figure 2: (A) Absorption spectra of thin (80 nm) and thick (500 nm) Ag_2S films. Inset: transmission electron microscopy (TEM) image of synthesized Ag_2S quantum dots (QDs) with the 5 nm scale plate. (B) High-resolution TEM image of Ag_2S QDs. (C) Energy-dispersive X-ray spectroscopy (EDS) of Ag_2S QDs thin film. (D) EDS of Ag_2S bulk target.

spectra of Ag_2S QDs thin films were in agreement with the tendency of the suspension, illustrating the QDs thin film we got. The linear increase with the absorption of different thickness suggests that amounts of Ag_2S QDs were absorbed after being spin-coated with different speeds, resulting in a buildup of homogeneous films. The inset in Figure 2A shows the transmission electron microscopy (TEM) image of Ag_2S QDs. The average size of QDs was ~4 nm (JEOL-JEM-2100F, Japan). High-resolution TEM image of Ag_2S QDs with well-developed lattice fringes shows good crystallinity of all the samples in Figure 2B. Atomic planes with *d*-spacing of 0.225 nm are indexed to the (122) facet of monoclinic α-Ag_2S, suggesting the synthesis of Ag_2S QDs. Energy-dispersive X-ray spectroscopy (EDS) (S-4800, Hitachi, Japan) was carried out to further characterize the composition of QDs. Ag and S elements were with an atomic ratio of 2.11:1 in the synthesized QDs, which is similar to the bulk Ag_2S (Figure 2C,D). So that the combined TEM and EDS results reveal that the thin film we manufactured was indeed Ag_2S QDs thin film. Figure 3 shows the CA Z-scans of two Ag_2S QD films using 30 fs pulses at $\lambda = 800$ nm. The pulse energy was 0.36 μJ. The maximum fluence at the beam waist during these Z-scans was 7×10^{-3} J cm^{-2} and the peak intensity was $I_0 = 2\times10^{11}$ W cm^{-2}.

In the general case of joint contribution of nonlinear refraction and absorption the normalized transmittance of samples along z-axis, $T(z)$, can be presented as follows [34]:

$$T(z) = 1 + \frac{4x}{(x^2+9)(x^2+1)}\Delta\Phi_0 - \frac{2(x^2+3)}{(x^2+9)(x^2+1)}\Delta\psi_0 \qquad (1)$$

where $\Delta\Phi_0 = k\gamma I_0 L_{eff}$ and $\Delta\psi_0 = \beta I_0 L_{eff}/2$ are the phase variations due to nonlinear refraction and nonlinear absorption, respectively, $x = z/z_0$, $z_0 = k(w_0)^2/2$ is the Rayleigh length, $k = 2\pi/\lambda$ is the wave number, w_0 is the beam waist radius at the $1/e^2$ level of intensity distribution, I_0 is the intensity in focal plane, $L_{eff} = [1-\exp(-\alpha_0 L)]/\alpha_0$ is the effective length of the medium, α_0 is the linear absorption coefficient, and L is the thickness of sample.

By making the substitution $\rho = \beta/2k\gamma$ one can get the relation between $\Delta\Phi_0$ and $\Delta\psi_0 (\Delta\psi_0 = \rho\Delta\Phi_0)$. In that case (1) can be re-written as follows:

$$T = 1 + \frac{2(-\rho x^2 + 2x - 3\rho)}{(x^2+9)(x^2+1)}\Delta\Phi_0 \qquad (2)$$

This formula was fitted with experimental CA data. The fitting of experimental curves allowed to extract phase changing due to the change of the refractive and

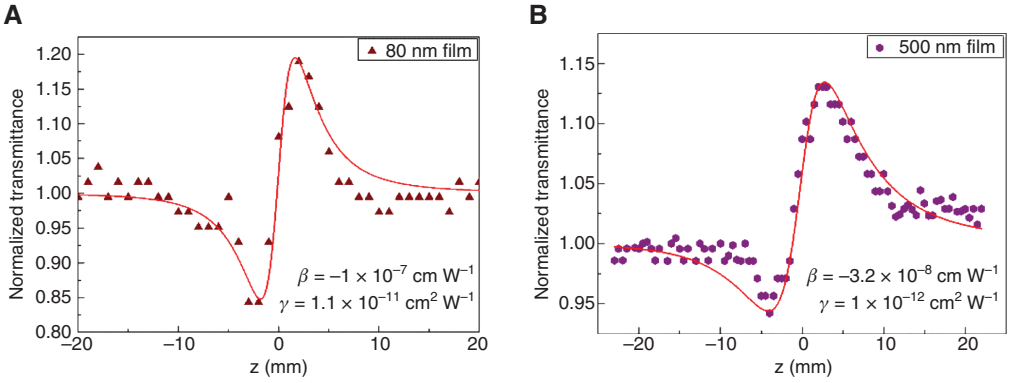

Figure 3: Z-scan measurements at 800 nm.
Closed aperture (CA) Z-scans of (A) 80 nm and (B) 500 nm thick films. Solid curves show the fits using (2).

absorptive properties of the transparent materials. The measurement of nonlinear refractive index and nonlinear absorption coefficients was based on the determination of phase change of probe pulses.

Thinner film had higher values of γ and β. The β values of the 80 and 500 nm films were measured to be -1×10^{-7} and -3.2×10^{-8} cm W^{-1}. The negative nonlinear absorption was attributed to saturable absorption (SA). The nonlinear refractive index of thicker film ($\gamma=1\times10^{-12}$ cm^2 W^{-1}) was 11 times smaller than that of the thin film ($\gamma=1.1\times10^{-11}$ cm^2 W^{-1}). Notice that the Z-scan measurements of the dissolved in the hexane Ag_2S QDs showed that the nonlinear absorption coefficient of this suspension at $\lambda=800$ nm was 8.8×10^{-12} cm W^{-1}, and the nonlinear refractive index was 3×10^{-16} cm^2 W^{-1} [35] that was correspondingly 10^4 and 10^5 times smaller than the same parameters of 80 nm film. Many reasons can account for the improved nonlinear absorption in the Ag_2S QDs thin films such as improved electronic passivation of the QDs surface, the smaller Ag_2S QDs size, contribution from Ag_2S two-photon absorption.

In the case of 400 nm, 30 fs probe pulses the nonlinear refraction was larger than in the case of 800 nm pulses. The CA Z-scan of 80 nm film showed the positive nonlinear refraction and positive nonlinear absorption, when the valley was deeper than the peak (Figure 4A). The nonlinear refraction index of this thin film was calculated to be $\gamma=3.3\times10^{-10}$ cm^2 W^{-1}, while in the case of thicker film (500 nm) it was 25 times smaller ($\gamma=1.3\times10^{-11}$ cm^2 W^{-1}).

For the OA Z-scans the normalized transmittance is given by [32]

$$T(z)=\sum_{m=0}^{\infty}\frac{\left[\dfrac{-\beta(I)I_0L_s^{\text{eff}}}{(1+(x)^2)}\right]^m}{(m+1)^{3/2}}, \tag{3}$$

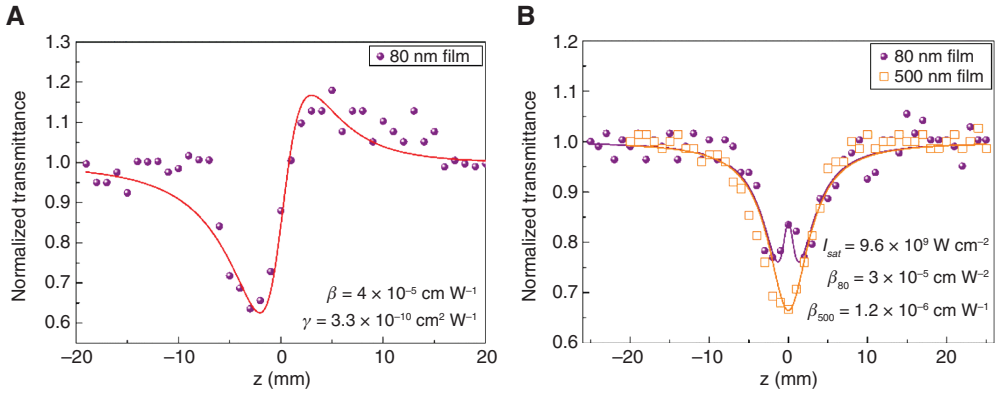

Figure 4: Z-scan measurement at 400 nm.
Normalized transmittances in the case of (A) CA Z-scan of 80 nm film and (B) Open-aperture (OA) Z-scans of 80 and 500 nm films measured using the 400 nm, 30 fs pulses. Theoretical curves are the fits deduced from Eqs. (2), (4), and (5).

This formula can be presented in a simplified form

$$T(z) \approx 1 - \frac{q}{2\sqrt{2}}, \tag{4}$$

where $q = \beta I_0 L_{\text{eff}} / (1 + z^2 / z_0^2)$.

In the case of SA, the nonlinear absorption coefficient and absorption coefficient are determined by the relations

$$\beta(I) = \frac{\alpha(I) - \alpha_0}{I}, \tag{5}$$

$$\alpha(I) = \alpha_0 \frac{1}{1 + \left(\frac{I}{I_{\text{sat}}}\right)} \tag{6}$$

Here I_{sat} is the saturation intensity for the SA, which is related with the concentration of the active centers in the medium, the effective cross-sections of involved transitions and the lifetimes of excited states. In the case of low intensity, the SA at $\lambda = 800$ nm dominated over other nonlinear optical processes in the used samples.

The fitting of the experimental data allows to extract a phase shift of the probe laser pulses. If the phase shift is positive (i.e. self-focusing occurs), then the peak will trail the valley. If the phase shift is negative, then the valley will trail the peak (i.e. self-defocusing). The magnitude of the phase shift can be determined from the change in normalized transmittance between peak and valley, ΔT_{pv}, using the relation

$$\Delta\Phi_0 = \frac{\Delta T_{\text{pv}}}{0.406\ (1 - S)^{0.27}}. \tag{7}$$

Here S is the fraction of beam transmitted through the aperture. The nonlinear index, n_2, can then be determined from phase change.

Contrary to the 800 nm probe pulses, the use of 400 nm radiation led to variation of nonlinear absorption from SA to reverse saturable absorption (RSA). The CA measurements revealed the high value of nonlinear absorption coefficient in the case of 80 nm film ($\beta = 4 \times 10^{-5}$ cm W^{-1}). Almost similar value was obtained during OA Z-scan of this film ($\beta = 3 \times 10^{-5}$ cm W^{-1}, Figure 4B). Note that simultaneously with this process we observed the growth of normalized transmittance at the highest intensities that can be attributed to the higher-order SA effect (see the variation of normalized absorption in the vicinity of $z = 0$, Figure 4B). The nonlinear absorption in thicker (500 nm) film ($\beta = 1.2 \times 10^{-6}$ cm W^{-1}, in the case of OA Z-scan, and $\beta = 1.6 \times 10^{-6}$ cm W^{-1}, in the case of CA Z-scan) was 25 times smaller compared with the β of thin film. The two positive γ values reveal that the Ag_2S QDs films show a self-focusing behavior at both 400 and 800 nm wavelengths. The β values are positive (at 400 nm) and negative (at 800 nm), indicating that the Ag_2S QDs thin film behave as strong excited-state absorbers and optical bleachers, respectively, at the corresponding wavelengths. The measured relaxation time of Ag_2S QDs thin films at 400 nm was short enough for them to be applied for optical switching devices.

In order to understand the observed difference in the Z-scan profile for Ag_2S QD thin film with different thickness, optical density of these films can provide the valuable reasoning. As reported in the literature, Ag_2S QD exhibit weak surface plasmon resonance at 440 nm. Moreover the excitation at 400 nm using moderate intensity of femtosecond laser pulses in our experiment suggest the nonlinear absorption originating from multiple excitons generation in single QD through nonradiative auger recombination process. However, the ground state bleaching (GSB) for the Ag_2S is already reported at 3.2 E_g for the Ag_2S QD by the Sun et al. [36], where E_g is the band gap energy. The GSB process leads to the increase in the transmittance as the intensity of laser pulse increases which occurs in the vicinity of the focal region. For thinner film of 80 nm, the threshold for the GSB happened to be smaller due to the density of the Ag_2S QD in the vicinity of the irradiated area whereas for thicker film of 500 nm, this threshold is much higher due to the number density of the Ag_2S QD. There are few reports on the Ag_2S nanocrystal (NC) in suspensions suggesting the two-photon absorption process at reasonably high fluence of incidence photons. The obtained β in Ag_2S QD was found to be much larger as compared to the Ag_2S NC at 532 nm ($\beta = 5.5 \times 10^{-8}$ cm W^{-1}, [37]).

There are various reports on the TA phenomenon in the Ag_2S QDs and NCs measured in the near-infrared region [36, 38], which was attributed to the Auger recombination process. Meantime, the decay time constant for Ag_2S QDs was reported neither at 800 nm nor at 400 nm wavelength regions. We measured the TA in the 80 and 500 nm thin films containing the Ag_2S QDs deposited on the glass substrates using the 400 nm, 30 fs pulses. The energy of the pump pulse was used to be 30 nJ to excite the films. Prior to the measurements of the TA of films, similar measurements of the glass substrate were performed, to separate its contribution from the TA data obtained in the case of Ag_2S QD thin films, which showed the absence of the change in transmittance with time delay in the case of substrates.

Figure 5A shows the temporal evolution of transmittance in the case of the 80 nm Ag_2S QD thin film. The TA profile demonstrated the transient bleaching due to SA as compared to the reverse process in the 500 nm thick Ag_2S QD film (Figure 5B). In the case of 500 nm Ag_2S QD film, transient transmittance decreases with delay time, which is due to RSA during the temporal overlap of pump and probe pulses. In order to confirm the RSA at 400 nm wavelength, we analyzed the OA Z-scans of these two films (Figure 4B), which depicted the positive nonlinear absorption at employed pulse energy and at the area out from the maximal intensity region (i.e. out from the focal area). However, as already mentioned, in the vicinity of focal area, the transmittance of laser pulses increased for 80 nm Ag_2S QD thin film, which is probably due to the dominance of SA phenomenon over RSA, contrary to the case of the 500 nm film showing the RSA at these conditions. Thus our TA measurements (Figure 5) were found to be consistent with the OA Z-scan studies of two films. The decay time constants were determined to be 150 and 245 fs in the case of 80 and 500 nm films respectively. The difference of the decay times for these two films was attributed to different life times of excited states and absorption probabilities in the case of thin and thick Ag_2S QD films.

3.2 HHG in the plasmas produced on the Ag_2S QD films

A search for new applications of QDs is an important task for the optical community. One of the ideas is to find the optimal conditions in application of such QDs as effective emitters of the high-order harmonics of femtosecond pulses for the development of the efficient sources of coherent XUV radiation. To study the high-order nonlinear optical properties through HHG the Ag_2S QD suspension was dried on the quartz substrates and placed in the vacuum chamber for creation of the plasma plume by laser ablation of this film. We analyzed the influence of the delay between the heating and the driving pulses and application of different energies of heating pulses on the harmonics yield.

Figure 6 shows the spectra of the high-order harmonics in the spectral range of 30–80 nm generated from the ablated QD thin film. The optimal delay between the heating and the driving pulses was found to be 400–500 ns. This figure also shows the plasma emission spectrum of ablated Ag_2S QD film. Note that the conditions of ablation at relatively high pulse energy of the heating radiation ($E_{ns} = 9$ mJ), when the plasma emission shown in Figure 6C dominates in the XUV spectra, are unsuitable for efficient HHG due to the presence of a large amount of free electrons, which prevent the maintenance of optimal phase relation between the generated harmonics.

Lesser excitation of the QD-containing films (by 3 and 5 mJ pulses) allowed formation of the plasmas suitable for HG (Figure 6A,B). Odd harmonics of 800 nm radiation up to the 23rd order (H23) were achieved using the Ag_2S QD plasmas. The appearance of strong harmonics emission did not coincide with the plasma emission from highly charged particles in the studied spectral range (30–80 nm) that confirmed that these experiments were carried out in a soft regime of ablation of QD-containing targets. The driving pulse [$I \approx (2\text{–}5) \times 10^{14}$ W cm^{-2}] did not cause the appearance of strong ionic emission from higher charged molecules and QDs as well.

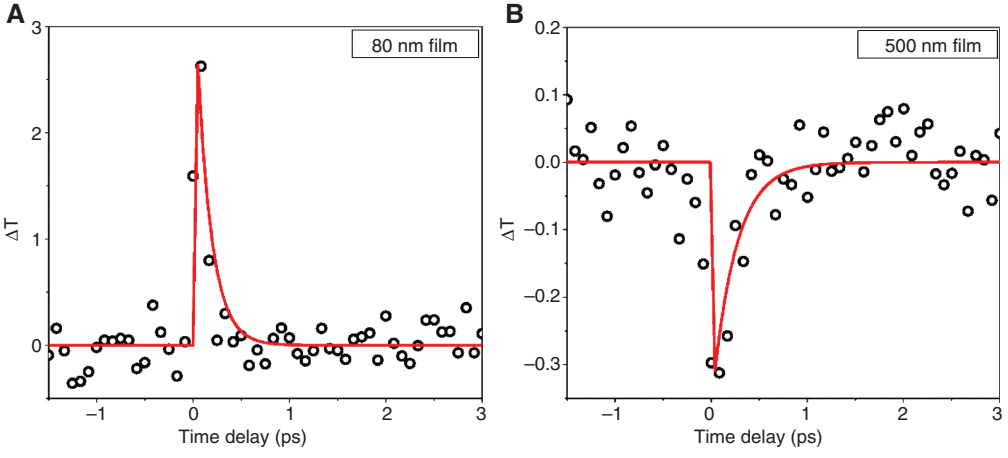

Figure 5: Temporal evolution of probe pulse transmittance through the Ag_2S films in the case of 400 nm, 30 fs pulses. (A) 80 nm thick film and (B) 500 nm thick film.

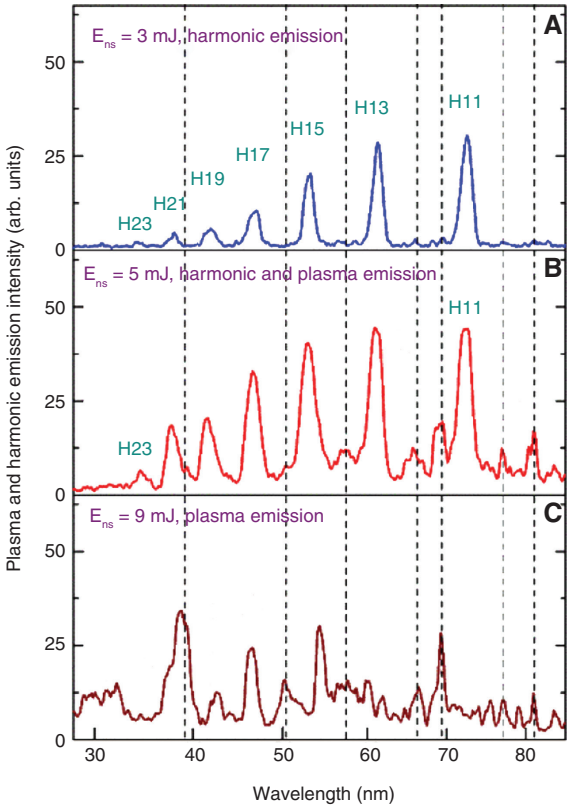

Figure 6: Harmonics emission spectrum.
(A) Harmonics emission spectrum in the case of Ag_2S QD ablation of thin films using 3 mJ, 5 ns pulses. (B) Harmonics emission spectrum in the case of Ag_2S QD ablation of thin films using 5 mJ, 5 ns pulses. (C) Plasma emission spectrum in the case of Ag_2S QD ablation of thin films using 9 mJ, 5 ns pulses. Dashed lines show the similarity in plasma emission lines in these three conditions of plasma formation.

The estimate of HHG conversion efficiency was carried out using the comparison with known results from other plasmas (silver and carbon [39, 40]). In the case of silver plasma at similar conditions of experiments, we observed the almost three times smaller conversion efficiency with regard to Ag_2S QD plasma. By knowing the conversion efficiency from previous measurements of harmonic generation in the plasmas produced on the surface of bulk Ag at similar experimental conditions (8×10^{-6} [39]) we deduced that HHG conversion efficiency in Ag_2S QD plasmas was ~2×10^{-5}.

The application of two electronically separated pulses from different lasers synchronized by a digital delay generator allows to analyze the involvement of various ablated species in the HHG process. Application of this approach for HHG in multi-particle plasmas, alongside with other methods of harmonic enhancement, requires the analysis of the ablated species, to temporally match them with the propagation of driving femtosecond pulses through the plasma.

The highest harmonics yield was observed in the plasmas of ablated Ag_2S QD thin film (atomic weight 247.8 amu) after 400–500 ns delay from the beginning of ablation. Note that the use of carbon plasma (atomic weight 12 amu) allowed maximal harmonic intensity after a significantly smaller delay (about 30–50 ns between the heating and the driving pulses using similar pulse energies). Further increase of the delay led to a gradual decrease of the HHG efficiency from Ag_2S QDs plasmas (see variations of 13th and 17th harmonic yields at different delays, Figure 7). The harmonics almost disappeared once the delay exceeded 2 µs. No harmonics were observed after the maximum delays explored in these studies (25 µs).

Experiments using ablated Ag_2S bulk target led to similar dependence of the harmonics yield on the delay between the heating and the driving pulses. These studies showed that, independently on whether molecules or QDs spread out from the target surface of the same material, they appear in the area of femtosecond beam propagation at approximately the same time. The harmonics cut-off was higher for the ablated bulk Ag_2S (H33) with regard to the QD species. Plasma from the ablated Ag_2S QD thin film allowed generation of up to H19 at similar experimental conditions of ablation (Figure 8). In the meantime, the conversion efficiency for the lowest orders in that case was three to four times larger compared with the ablation of bulk Ag_2S. For the QDs thin films have a higher intensity of the harmonic generation within 500 ns than the same bulk material. The HHG during ablation of QDs-containing targets has revealed the advantages of using such species for frequency conversion in the XUV range. Due to the

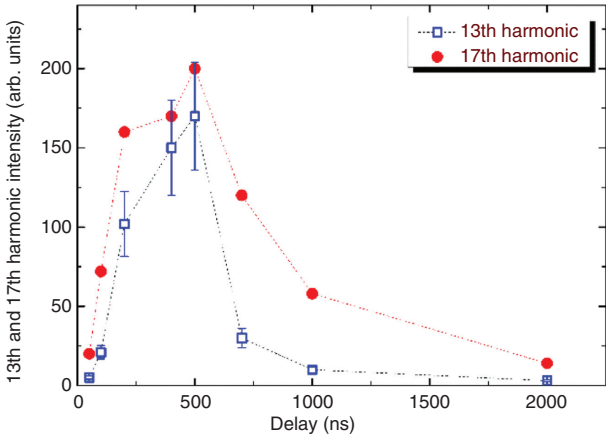

Figure 7: The 13th and the 17th harmonics emission variations at different delays between heating nanosecond pulses and driving femtosecond pulses.

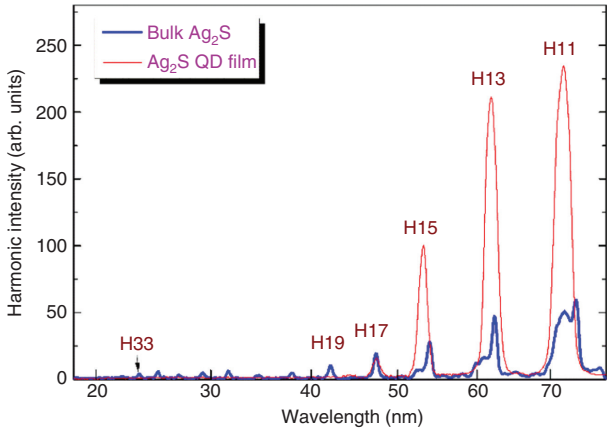

Figure 8: Comparison of harmonics spectra in the case of ablation of the Ag_2S bulk target (thick curve) and Ag_2S QD thin film (thin curve).

larger cross-section of recombination, possibility of recombination of accelerated electron with parent multi-atomic particles through either recombination with the same atom or the neighbor atom and the multi-atomic particle as a whole were considered as the most probable reasons in the growth of HHG yield from such plasmas. However, the conditions of experiments, particularly the delay between heating and driving pulses, were not optimized.

The developed method for the analysis of multi-particle plasma formation using two laser sources for HHG using laser ablation can be considered a promising approach for materials science. Its application will expand the possibilities of optimizing HHG in laser-produced plasma plumes, allow to implement new approaches for the study of large molecules and clusters undergoing ablation, and significantly increase the range of the objects of study compared with HHG in gases.

4 Conclusions

In this paper, the results of nonlinear optical studies of Ag_2S QD thin films are presented. Using the OA and CA Z-scan technique and theoretical fitting, we calculated the nonlinear absorption coefficient to be 4×10^{-5} cm W^{-1} for the 80 nm thick film in the case of 400 nm probe pulses. The nonlinear absorption coefficients and nonlinear refractive indices of 80 and 500 nm thick films were significantly larger than for the Ag_2S QDs suspension. In the case of TA measurements the two distinct characteristic time constants of 150 and 245 fs were obtained for the films of different thickness. We also investigated the high harmonics emission from the ablation of 80 nm films using two laser sources. The conversion efficiency in the plasmas produced by ablation of the Ag_2S QD thin film (2×10^{-5}) was several times higher compared to the case of bulk Ag_2S ablation. Our approach establishes a novel and efficient way of generating high-order harmonic yield.

Acknowledgments: R.A.G. thanks the financial support from Chinese Academy of Sciences President's International Fellowship Initiative (Grant No. 2018VSA0001).

Funding: National Key Research and Development Program of China (2017YFB1104700, 2018YFB1107202), Natural Science Foundation of China (91750205, 61774155, 61705227), Jilin Provincial Science & Technology Development Project (20180414019GH), Russian Fund for Basic Research (RFBR Grant № 17-52-12034 ННИО_а).

References

[1] Yarema M, Pichler S, Sytnyk M, et al. Infrared emitting and photoconducting colloidal silver chalcogenide nanocrystal quantum dots from a silylamide-promotedsynthesis. ACS Nano 2011;5:3758–65.
[2] Jiang P, Zhu CN, Zhang ZL, Tian ZQ, Pang DW. Water-soluble Ag_2S quantum dots for near-infrared fluorescence imaging in vivo. Biomaterials 2012;33:5130–5.
[3] Hwang I, Seol M, Kim H, Yong K. Improvement of photocurrent generation of Ag_2S sensitized solar cell through co-sensitization with CdS. Appl Phys Lett 2013;103:023902.
[4] Hwang I, Yong K. Environmentally benign and efficient Ag_2S-ZnO nanowires as photoanodes for solar cells: comparison with CdS-ZnO nanowires. Chemphyschem 2013;14:364–8.
[5] Gao X, Cui Y, Levenson RM, Chung LWK, Nie S. In vivo cancer targeting and imaging with semiconductor quantum dots. Nat Biotechnol 2004;22:969.
[6] Dubertret B, Skourides P, Norris DJ, Noireaux V, Brivanlou AH, Libchaber A. In vivo imaging of quantum dots encapsulated in phospholipid micelles. Science 2002;298:1759.
[7] de Nalda R, Lopez-Arias M, Sanz M, Oujja M, Castillejo M. Harmonic generation in ablation plasmas of wide bandgap semiconductors. Phys Chem Chem Phys 2011;13:10755–61.
[8] Junod P, Hediger H, Kilchör B, Wullschleger J. Metal-non-metal transition in silver chalcogenides. Philos Mag 1977;36:941–58.
[9] Linnenbank H, Grynko Y, Förstner J, Linden S. Second harmonic generation spectroscopy on hybrid plasmonic/dielectric nanoantennas. Light Sci Appl 2016;5:e16013.
[10] Gao L, Chen C, Zeng K, et al. Broadband, sensitive and spectrally distinctive SnS2 nanosheet/PbS colloidal quantum dot hybrid photodetector. Light Sci Appl 2016;5:e16126.
[11] Abe S, Joos JJ, Martin LIDJ, Hens Z, Smet PF. Hybrid remote quantum dot/powder phosphor designs for display backlights. Light Sci Appl 2017;6:e16271.
[12] Disney CER, Pillai S, Johnson CM, Green MA. Self-assembled nanostructured rear reflector designs for thin-film solar cells. ACS Photonics 2015;2:1108–16.

[13] Kuang P, Eyderman S, Hsieh M-L, Post A, John S, Lin S-Y. Achieving an accurate surface profile of a photonic crystal for near-unity solar absorption in a super thin-film architecture. ACS Nano 2016;10:6116–24.
[14] Oskooi A, De Zoysa M, Ishizaki K, Noda S. Experimental demonstration of quasi-resonant absorption in silicon thin films for enhanced solar light trapping. ACS Photonics 2014;1:304–9.
[15] Ganeev RA, Baba M, Morita M, et al. Nonlinear optical properties of CdS and ZnS nanoparticles doped into zirconium oxide films. J Opt A 2004;6:447.
[16] Karali T, Can N, Valberg L, et al. Optical properties and luminescence of metallic nanoclusters in ZnO:Cu. Phys B 2005;363:88–95.
[17] Ganeev RA, Chakravarty U, Naik PA, et al. Pulsed laser deposition of metal films and nanoparticles in vacuum using subnanosecond laser pulses. Appl Opt 2007;46:1205–10.
[18] Ovchinnikov OV, Smirnov MS, Perepelitsa AS, Shatskikh TS, Shapiro BI. Optical power limiting in ensembles of colloidal Ag_2S quantum dots. Quantum Electron 2015;45:1143–50.
[19] Aleali H, Mansour N. Nanosecond high-order nonlinear optical effects in wide band gap silver sulfide nanoparticles colloids. Optik 2016;127:2485–9.
[20] Karimzadeh R, Aleali H, Mansour N. Thermal nonlinear refraction properties of Ag_2S semiconductor nanocrystals with its application as a low power optical limiter. Opt Commun 2011;284:2370–5.
[21] Brabec T, Krausz F. Intense few-cycle laser fields: frontiers of nonlinear optics. Rev Mod Phys 2000;72:545–91.
[22] Schafer KJ, Yang B, DiMauro LF, Kulander KC. Above threshold ionization beyond the high harmonic cutoff. Phys Rev Lett 1993;70:1599–602.
[23] Lenzner M, Krüger J, Sartania S, et al. Femtosecond optical breakdown in dielectrics. Phys Rev Lett 1998;80:4076–9.
[24] Apostolova T, Obreshkov B. High harmonic generation from bulk diamond driven by intense femtosecond laser pulse. Diam Relat Mater 2018;82:165–72.
[25] Luu TT, Garg M, Kruchinin SY, Moulet A, Hassan MT, Goulielmakis E. Extreme ultraviolet high-harmonic spectroscopy of solids. Nature 2015;521:498.
[26] Ghimire S, DiChiara AD, Sistrunk E, Agostini P, DiMauro LF, Reis DA. Observation of high-order harmonic generation in a bulk crystal. Nature Phys 2011;7:138.
[27] Ganeev RA, Suzuki M, Baba M, Ichihara M, Kuroda H. High-order harmonic generation in Ag nanoparticle-containing plasma. J Phys B 2008;41:045603.
[28] Ganeev RA, Suzuki M, Baba M, Ichihara M, Kuroda H. Low- and high-order nonlinear optical properties of $BaTiO_3$ and $SrTiO_3$ nanoparticles. J Opt Soc Am B 2008;25:325–3.
[29] Ganeev RA, Naik PA, Singhal H, et al. High-order harmonic generation in carbon-nanotube-containing plasma plumes. Phys Rev A 2011;83:013820.
[30] Ganeev RA, Strelkov VV, Hutchison C, et al. Experimental and theoretical studies of two-color-pump resonance-induced enhancement of odd and even harmonics from a tin plasma. Phys Rev A 2012;85:023832.
[31] Kayanuma Y. Quantum-size effects of interacting electrons and holes in semiconductor microcrystals with spherical shape. Phys Rev B 1988;38:9797–805.
[32] Sheik-Bahae M, Said AA, Wei TH, Hagan DJ, Van Stryland EW. Sensitive measurement of optical nonlinearities using a single beam. IEEE J Quant Elect 1990;26:760–79.
[33] Gui R, Sun J, Liu D, Wang Y, Jin H. A facile cation exchange-based aqueous synthesis of highly stable and biocompatible Ag_2S quantum dots emitting in the second near-infrared biological window. Dalton T 2014;43:16690–7.
[34] Liu X, Guo S, Wang H, Hou L. Theoretical study on the closed-aperture Z-scan curves in the materials with nonlinear refraction and strong nonlinear absorption. Opt Commun 2001;197:431–7.
[35] Fu Y, Ganeev RA, Zhao C, et al. Ag_2S quantum dots in the fields of picosecond and femtosecond UV and IR pulses: optical limiting, nonlinear absorption and refraction properties. Appl Phys B 2018;125:1.
[36] Sun J, Yu W, Usman A, et al. Generation of multiple excitons in Ag_2S quantum dots: single high-energy versus multiple-photon excitation. J Phys Chem Lett 2014;5:659–5.
[37] Mir WJ, Swarnkar A, Sharma R, Katti A, Adarsh KV, Nag A. Origin of unusual excitonic absorption and emission from colloidal Ag_2S nanocrystals: ultrafast photophysics and solar cell. J Phys Chem Lett 2015;6:3915–22.
[38] Chand S, Sharma E, Sharma P. Phase change induced quantization in NIR emitting Ag_2S nanocrystals: structural and optical response for solar energy applications. J Alloy Compd 2019;770:1173–80.
[39] Ganeev RA, Baba M, Suzuki M, Kuroda H. High-order harmonic generation from silver plasma. Phys Lett A 2005;339:103–9.
[40] Ganeev RA, Hutchison C, Witting T, et al. High-order harmonic generation in graphite plasma plumes using ultrashort laser pulses: a systematic analysis of harmonic radiation and plasma conditions. J Phys B 2012;45:165402.